

Article

Neutral and Ionic Form of (Benzylthio)Acetic Acid in Novel Aminopyrimidine Based Multi-Component Crystalline Phases

Justyna Sienkiewicz-Gromiuk ^{1,*}  and Aleksandra Drzewiecka-Antonik ²

¹ Department of General and Coordination Chemistry and Crystallography, Institute of Chemical Sciences, Faculty of Chemistry, Maria Curie-Skłodowska University in Lublin, M. Curie-Skłodowska Sq. 2, 20-031 Lublin, Poland

² Institute of Physics, Polish Academy of Sciences, Aleja Lotnikow 32/46, 02-668 Warsaw, Poland; adrzew@ifpan.edu.pl

* Correspondence: justyna.sienkiewicz-gromiuk@mail.umcs.pl

Abstract: (benzylthio)acetic acid (HBTA) and some aminopyrimidines, namely 2-aminopyrimidine (2-AP), 5-aminopyrimidine (5-AP), 2-amino-4,6-dimethylpyrimidine (2-A-4,6-DMP), and 2,4,6-triaminopyrimidine (2,4,6-TAP), were successfully embodied as structural units into the construction of a total of four novel supramolecular organic frameworks. The received crystalline solids were inspected by single-crystal X-ray diffraction (SC XRD) in order to obtain insight into the structural and supramolecular facets. The SOFs deriving from 2-AP, 5-AP, and 2-A-4,6-DMP crystallize in the form of co-crystals (1–3), while the one originating from 2,4,6-TAP crystallizes as a salt solvate (4). The SC XRD results indicated the different contents of structural residues present in the asymmetric units of the crystals 1–4 despite using the same molar ratio of molecular co-former components in each case. The molecular structures of co-crystals 1–3 consist of either one neutral residue of each starting component (1 and 3) or one nonionized residue of the aminopyrimidine ingredient and two neutral residues of the acidic component (2). The asymmetric unit of salt solvate 4 is composed of two ionized residues of each co-former (two 2,4,6-TAP⁺ cations and two BTA[−] anions) and one MeOH solvent molecule. The most extensive H-bonding network is observed in the crystal structure of salt solvate 4. The relevant molecular ingredients in co-crystals 1–3 are mainly held together by the neutral O_{carboxylic}–H···N_{pyrimidine} and N_{amine}–H···O_{carboxylic} H-bonds. In the case of aggregate 4, the corresponding ionic residues are predominantly sustained by the charged-assisted N_{pyrimidinium}–H···O_{carboxylate} and N_{amine}–H···O_{carboxylate} hydrogen interactions. The MeOH solvent, incorporated into the crystal lattice of adduct 4, is also involved in H-bonding by simultaneously serving as the single donor in O_{MeOH}–H···S and the single acceptor in N_{amine}–H···O_{MeOH} H-bonds, which afforded the structural diversity within the 2,4,6-TAP⁺ cations and BTA[−] anions. Other weaker sets of additional non-covalent contacts existing in the crystal structures of analyzed conglomerates are involved in the self-assembly, stabilization, and expansion of total supramolecular organic frameworks. The fact of the formation of non-covalent bonded supramolecular organic frameworks in question is also reflected in corresponding results obtained through elemental analysis (EA), Fourier transform infrared spectroscopy (FT-IR), and thermal analysis (TG/DSC).

Keywords: (benzylthio)acetic acid; aminopyrimidines; supramolecular organic frameworks (SOFs); co-crystal; salt solvate; nonbonding contacts; SC XRD structural analysis; FT-IR spectroscopy; thermal study



Citation: Sienkiewicz-Gromiuk, J.; Drzewiecka-Antonik, A. Neutral and Ionic Form of (Benzylthio)Acetic Acid in Novel Aminopyrimidine Based Multi-Component Crystalline Phases. *Crystals* **2023**, *13*, 1628. <https://doi.org/10.3390/cryst13121628>

Academic Editor: Josefina Perles

Received: 28 October 2023

Revised: 18 November 2023

Accepted: 21 November 2023

Published: 23 November 2023



Copyright: © 2023 by the authors. Licensee MDPI, Basel, Switzerland. This article is an open access article distributed under the terms and conditions of the Creative Commons Attribution (CC BY) license (<https://creativecommons.org/licenses/by/4.0/>).

1. Introduction

Supramolecular organic frameworks (SOFs), also known as multi-component crystalline solids/phases or multi-component molecular crystals, are a group of materials fabricated using supramolecular crystal engineering [1]. The supramolecular conglomerates are formed as a result of spontaneous intermolecular self-assembling achieved by

creating various bunches of non-covalent interactions between the favorable functional groups that build up the molecules of organic co-partners [2]. The occurrence of the different non-covalent contacts, embracing classical and nonclassical H-bonds, electrostatic forces, $\pi\cdots\pi$ stacking, π -cation and π -anion, lone pair- π attractions, and others, is a necessary factor to direct the molecular arrangement in the crystals [3]. The process of intermolecular association based on the development of a combination of classical H-bonds and complementary weak non-covalent forces is responsible for the fabrication of specific crystal structures bearing particular physicochemical properties [4].

The carboxylic acids and basic *N*-heterocyclic derivatives are very often employed in crystal engineering as effective building tectons in the production of new supramolecular organic frameworks (SOFs). Their leader position as building bricks in the process of engendering the multi-component organic crystalline phases is dictated by their chemical composition characterized by bearing excellent donor and acceptor moieties susceptible to effective organic acidic:basic supramolecular complexation. The most important functional group of organic acids, which strongly interacts with other organic partners with a basic nature, is the -COOH group. Acidic–basic supramolecular aggregation is carried out by the facilitated formation of the neutral $N-H\cdots O/O-H\cdots N$ or charged-assisted $N^+-H\cdots O^-$ and $N-H\cdots O^-$ H-bonds enclosed between pyrimidine/amine groups equipped with the lone electron pair localized on the nitrogen atoms of base ingredients and complementary carboxylic/carboxylate groups derived from acidic co-formers. These neutral or charged-assisted strong H-bonds, holding the acidic and basic components together, influence the crystalline form of the resulting multi-component molecular materials in the co-crystal/salt category. An introduction of the extra potential binding spacers (CH, CH₂, CH₃, aryl core, halogens, OH, S, O, SO₂, and NO₂) into the chemical structure of implemented co-partners yielded the more complicated networks of non-covalent forces that ultimately cause changes in the crystal packing, as well as features of supramolecular solids [5–7].

A literature survey unveiled that aminopyrimidine compounds have been filed to supramolecular complexation with large numbers of carboxylic acids. The selected aminopyrimidines (Figure 1), like 2-AP, 5-AP, 2-A-4,6-DMP, and 2,4,6-TAP, fit perfectly into generating the non-covalent bonding with various acidic derivatives due to the presence of three or five basic nitrogen sites.

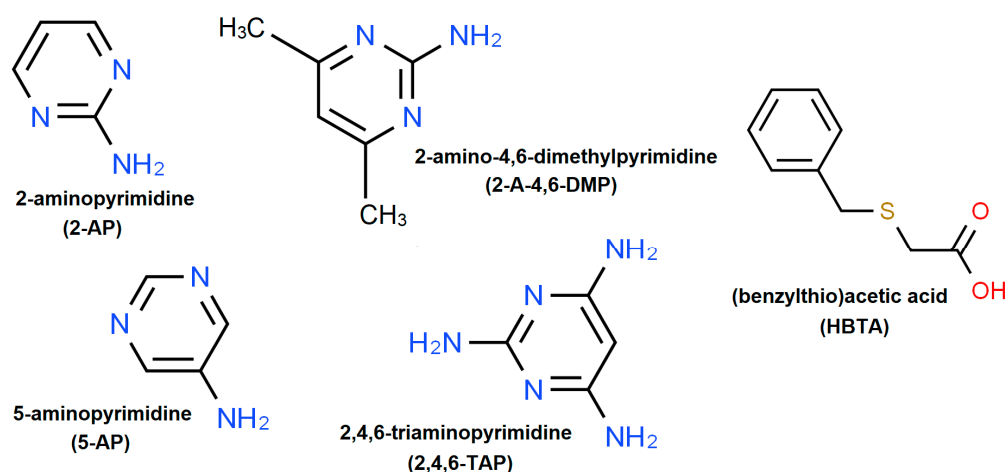


Figure 1. Chemical formulas of selected H-bond building blocks.

The CSD analysis [8] based on *ConQuest 2022.3.0* software [9] showed that the 2-AP and 2-A-4,6-DMP interact most readily with carboxylic co-partners giving 64 and 58 multi-component molecular crystals, respectively (Figure 2A). The 2,4,6-TAP was enclosed in 23 supramolecular architectures, whereas no data regarding the utility of 5-AP as a building brick in supramolecular complexation were found (Figure 2A). The 2-AP, as well as 2-A-4,6-DMP, remain in their neutral figure in the majority of disclosed

crystal structures obtained with the participation of carboxylic co-formers, which constitute 64.1% and 67.2% of the total number of acid:base supramolecules, respectively. The structural results published in the CSD database [8,9] and gathered in Figure 2B indicate that solely the 2-A-4,6-DMP entity builds the supramolecular complexes within all specified subclasses of multi-component crystalline phases [10].

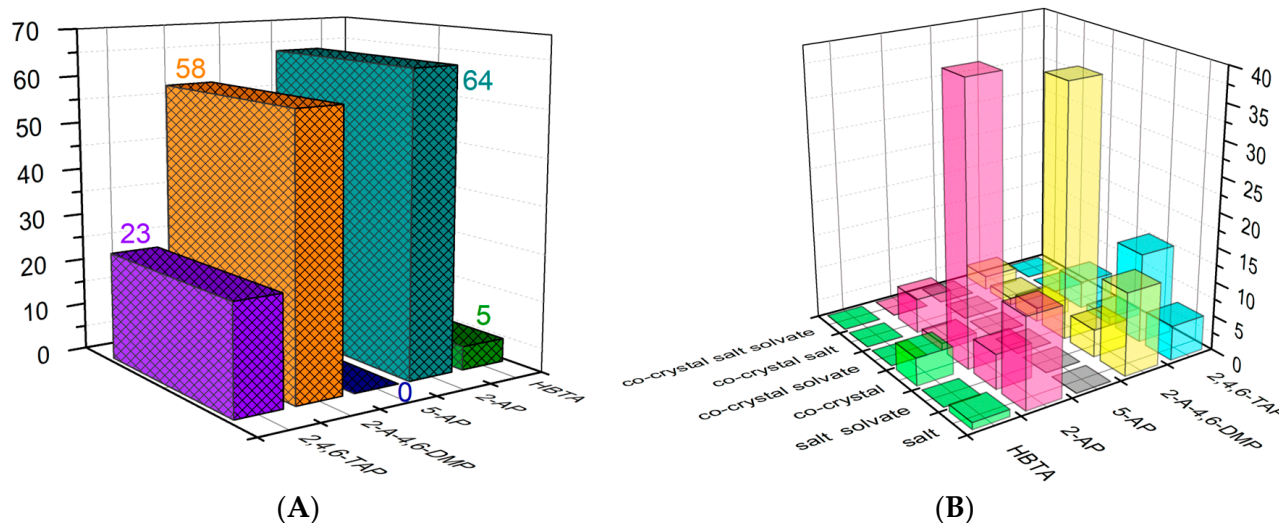


Figure 2. The number of reported crystal structures (A) along with the summary of crystalline forms (B) of multi-component molecular crystals containing HBTA:*N*-heterocycles as well as carboxylic acids: 2-AP/2-A-4,6-DMP/2,4,6-TAP synthons, respectively.

The supramolecular conglomerates fabricated from 2-AP and carboxylic co-partners generate two- or three-component molecular crystals belonging to almost all defined subclasses of SOFs [10], except the salt co-crystal solvate (Figure 2B). The 2-AP generally forms supramolecular adducts without any solvent as evidenced by only six reported acid:base crystalline solids containing solvent residues in the form of water (CSD refcode: NAXSIQ [11], PUDGRUF [12]/PUDGRUF01 [13], SUYQAF [14], and VEVNEQ [15]), ethanol (CSD refcode: AJECIB [16]), or nitrobenzene (CSD refcode: KAHMOV [17]). Interestingly, the supramolecular associations proceeding between 2-AP and benzoic acid resulted in the production of three co-crystal polymorphs described by *Pnma* (CSD refcode: NUKWEW [18] and NUKWEW01 [18]) and $P2_1/n$ (NUKWOG [18]) symmetry. The conformational discrepancies observed within the group of free dichloro-substituted phenoxyacetic acid derivatives influenced the crystal packing generated for their supramolecular adducts with 2-AP [19,20]. The inclusion of the specific isomer of dichloro-substituted phenoxyacetic derivatives caused different spatial arrangements of the structural residues included in the multi-component molecular crystals, namely *P*-1 (CSD refcode: LEWRIO [19]), $P2_1/n$ (CSD refcode: LEWREK [19]), $P2_1/c$ (CSD refcode: RADGEJ [20]), and *Pbcn* (RADFEI [20]) for 3,4-, 2,4-, 2,3- and 2,6-dichlorophenoxyacetic units, respectively.

The greatest structural diversity of 2-A-4,6-DMP-based supramolecular associations (Figure 2B) is demonstrated in relation to *p*-xylylene-bis(thioacetic) acid resulting in orthorhombic *Cmca* (CSD refcode: BOQNUS [21]) and monoclinic $P2_1/c$ (CSD refcode: BOQNIG [21]) co-crystals, as well as monoclinic $P2_1/c$ (CSD refcode: BOQNOM [21]) co-crystal monohydrate containing only the neutral $N-H\cdots O$ and $O-H\cdots N$ H-bonds. The 2-A-4,6-DMP is characterized by the most flexible behavior towards carboxylic acids so that as many as four-component crystalline solids are created. The 2-A-4,6-DMP and carboxylic co-formers present in the crystal lattices of the produced four-component supramolecules adopt the different residue types. The four-component co-crystal solvate formed between 2-A-4,6-DMP and ferulic acid (CSD refcode: JACCIC [22]) with the

participation of acridine and acetonitrile as the solvent contains all four structural units in their starting neutral figure. In the asymmetric unit of the other four-component crystal generated from 2-A-4,6-DMP and 2-hydroxy-6-naphthoic acid (CSD refcode: VAJQAB [23]), besides one water molecule, the 2-A-4,6-DMP⁺ monocation as well as both the monoanionic and neutral forms of 2-hydroxy-6-naphthoic acid are also observed. The reverse content of acidic:basic residues, found in the molecular structure of a four-component solid fabricated from 2-A-4,6-DMP and 5-aminoisophthalic acid (CSD refcode: POVXEG [24]), existed as the salt co-crystal hemihydrate, which consists of half of a water molecule, one monoanion of the acidic component, and both the monocationic and neutral forms of the basic ingredient.

In 78.3% of the published cases (Figure 2B), 2,4,6-TAP agents interact with carboxylic co-formers mostly by accepting the acidic proton by the *N*-heterocyclic nitrogen atom and becoming the 2,4,6-TAP⁺ cation. The 2,4,6-TAP⁺ residues in these crystals are always sustained with complementary carboxylates via the charge-assisted N⁺–H···O[−] and multiple N–H···O[−] H-bonds giving the supramolecular conglomerates in the form of salt solvates/hydrates (CSD refcode: CALVES [8,9], EPUQAK [25], GIFWOL [26], KEVLUV [27], KOCJAR [28], KOCHIX [28], KOCHOD [28], VEXQEX [29], VEXQOH [29], VEXQUN [29], VEQZOQ [29], VEXZUW [29], and VEYBAF [29]) and salts (CSD refcode: DARMIV [30], TESRAM [31], VEYBEJ [29], VIPZUS [8,9], and YUKVAE [32]). The 2,4,6-TAP also interacts with the acidic components only by the neutral O–H···N/N–H···O H-bonds, confirming the lack of proton transfer from the carboxylic unit to the 2,4,6-TAP entity (Figure 2B). The neutral H-bonds were observed in several 2,4,6-TAP:carboxylic SOFs appearing in the form of co-crystal (CSD refcode: SOVNIA [33]) or co-crystal solvates/hydrates (CSD refcode: SOVLAQ [33], SOVMOF [33], SOVQAV [33], and SOVQEZ [33]).

The acidic HBTA component [34], owing to its chemical structure (Figure 1) containing the –COOH group, organic sulphide –S– unit, –CH₂– spacers, and an aryl core, seems to be excellent under non-covalent contacts. So far, HBTA was exploited only in the construction of five supramolecular conglomerates (Figure 2A) with proline compounds (CSD refcode: XITMEW [35], XITMIA [35], and XITMOG [35]) isonicotinamide (CSD refcode: XITMUM [35]), as well as tryptamine (CSD refcode: XITNAT [35]). The designated X-ray crystal structures of HBTA-based supramolecular frameworks show that the acidic ingredient takes either a neutral or monoanion form (Figure 2B).

This paper is devoted to successful supramolecular self-assembly explained by the non-covalent interactions formed between the HBTA and the selected aminopyrimidines, such as 2-AP, 5-AP, 2-A-4,6-DMP, and 2,4,6-TAP, carried out through solution co-crystallization. This work also aims to characterize the generated organic complexes in the structural and supramolecular aspects utilizing SC X-ray crystallography to determine their spectral and thermal behavior by applying FT-IR spectroscopy and thermal analysis. Moreover, the incorporation of the 5-AP co-former into the process of supramolecular association with HBTA contributed to obtaining the 5-AP:carboxylic multi-component crystalline phase for the first time.

2. Materials and Methods

The co-formers and solvents used in co-crystallization experiments were commercial products without further purification. HBTA (purity 97%) was sourced from Sigma-Aldrich (St. Louis, MO, USA). 2-AP and 5-AP of analytical grade were purchased from Fluorochem Ltd (Hadfield, UK). 2-A-4,6-DMP (purity 98%) was received from Alfa Aesar GmbH (Karlsruhe, Germany), whereas 2,4,6-TAP (purity 97%) was procured from Acros Organics B.V.B.A (Geel, Belgium). The short-chained alcohols (methanol and ethanol) were provided by Avantor Performance Materials Poland S.A. (formerly POCH S.A.) (Gliwice, Poland).

2.1. Single Crystal Preparation by Solution Co-Crystallization

The crystals of novel multi-component molecular materials 1–4 were afforded under solution co-crystallization based on the slow solvent evaporation method at ambient condi-

tions. The well-shaped single crystals of new supramolecular complexes were successfully harvested in co-crystallization trials, in which the equimolar amounts of particular acidic and basic co-formers were combined with each other, and methanol or ethanol was applied as a solvent.

All SOFs were synthesized according to the same general procedure: A methanol or ethanol solution (5 mL) of HBTA (0.182 g, 1 mmol) was combined with the methanol or ethanol solution containing dissolved 1 mmol of individual *N*-containing compound (0.095 g of 2-AP and 5-AP, 0.123 g 2-A-4,6-DMP, or 0.125 g of 2,4,6-TAP) and stirred for 5 min. The resulting mixtures were then left undisturbed to evaporate naturally at an ambient temperature. Then, after several days, the well-shaped single crystals suitable for SC XRD analysis were harvested. The physical parameters of grown single crystals, namely the color, shape, and crystal size, are gathered in Table 1.

Adduct [2-AP·HBTA] (1)

Yield for 1: 0.251 g (90.61%); Elemental analysis results for $[C_4H_5N_3 \cdot C_9H_{10}O_2S]$ (MW: 277.34 g mol⁻¹). Calcd (%): C, 56.30; H, 5.45; N, 15.15; S, 11.56. Found (%): C, 56.61; H, 5.34; N, 15.28; S, 11.39.

Architecture [5-AP·2(HBTA)] (2)

Yield for 2: 0.228 g (82.31%); Elemental analysis results for $[C_4H_5N_3 \cdot 2(C_9H_{10}O_2S)]$ (MW: 459.56 g mol⁻¹). Calcd (%): C, 57.50; H, 5.48; N, 9.14; S, 13.95. Found (%): C, 57.32; H, 5.57; N, 9.31; S, 14.06.

Association [2-A-4,6-DMP·HBTA] (3)

Yield for 3: 0.285 g (93.44%); Elemental analysis results for $[C_6H_9N_3 \cdot C_9H_{10}O_2S]$ (MW: 305.39 g mol⁻¹). Calcd (%): C, 58.99; H, 6.27; N, 13.76; S, 10.50. Found (%): C, 59.17; H, 6.15; N, 13.62; S, 10.74.

Assembly [2(2,4,6-TAP⁺)·2(BTA⁻)·MeOH] (4)

Yield for 4: 0.269 g (87.62%); Elemental analysis results for $[2(C_4H_8N_5) \cdot 2(C_9H_9O_2S) \cdot CH_4O]$ (MW: 646.79 g mol⁻¹). Calcd (%): C, 50.14; H, 5.92; N, 21.66; S, 9.91. Found (%): C, 50.02; H, 5.81; N, 21.84; S, 10.08.

2.2. Single-Crystal X-ray Diffraction

An Oxford Diffraction Xcalibur CCD diffractometer (Oxford Diffraction Ltd., Abingdon, UK) equipped with a graphite-monochromated MoK_α radiation source ($\lambda = 0.71073 \text{ \AA}$) was employed to collect the single-crystal diffraction data for suitably selected crystals of complexes 1–4. The SC XRD measurements were carried out either at low-temperature conditions (100(2) or 120(2) K) or at an ambient temperature (295(2) K). The datasets were gathered using the ω scan technique with an angular scan width of 1.0°. The *CrysAlis Pro* [36] program was used for data acquisition, cell refinement, data reduction, and multi-scan absorption correction. The structures were solved by direct methods with *SHELXS-86* [37] and refined on F^2 by full-matrix least-squares techniques with *SHELXL-2018/3* [38] both implemented in *WinGX 2021.1* [39] software. Non-hydrogen atoms were refined with anisotropic displacement parameters. Hydrogen atoms were positioned geometrically (for carbon atoms) and were located from the different Fourier maps (for oxygen and nitrogen heteroatoms) and refined as riding atoms with isotropic displacement parameters. The molecular and crystal structure graphics were presented owing to the *Mercury 2022.3.0* program [40].

CCDC 2304064–2304067 contains the supplementary crystallographic data for this paper. The summary of crystal data, experimental details, and refinement results of structures in question are summarized in Table 1, whereas the geometry of intermolecular interactions existing in crystals 1–4 is shown in Table 2.

Table 1. Summary of X-ray crystallographic data for co-crystals 1–3 and salt solvate 4.

Compound	1 [2-AP·HBTA]	2 [5-AP·2(HBTA)]	3 [2-A-4,6-DMP·HBTA]	4 [2(2,4,6-TAP ⁺)·2(BTA ⁻)·MeOH]
Chemical formula	[C ₄ H ₅ N ₃ ·C ₉ H ₁₀ O ₂ S]	[C ₄ H ₅ N ₃ ·2(C ₉ H ₁₀ O ₂ S)]	[C ₆ H ₉ N ₃ ·C ₉ H ₁₀ O ₂ S]	[2(C ₄ H ₈ N ₅ ⁺)·2(C ₉ H ₉ O ₂ S ⁻)·CH ₃ OH]
Formula weight	277.34	459.58	305.39	646.79
T [K]	120(2)	100(2)	295(2)	120(2)
Crystal system	triclinic	monoclinic	triclinic	triclinic
Space group	<i>P</i> -1	<i>I</i> 2/ <i>a</i>	<i>P</i> -1	<i>P</i> -1
<i>a</i> [Å]	5.473(2)	11.2873(8)	7.3644(9)	11.9766(12)
<i>b</i> [Å]	8.720(3)	9.1219(6)	8.2883(10)	12.2477(11)
<i>c</i> [Å]	14.262(4)	22.7196(17)	13.5264(12)	12.7081(12)
α [°]	83.08(3)	90.00	82.748(9)	99.661(8)
β [°]	82.62(3)	103.110(7)	87.375(9)	111.581(9)
γ [°]	80.40(3)	90.00	75.153(10)	106.054(8)
<i>V</i> [Å ³]	662.1(4)	2278.3(3)	791.60(16)	1588.2(3)
<i>Z</i>	2	8	2	2
<i>D</i> _{calc.} [g cm ⁻³]	1.391	1.340	1.281	1.352
μ [mm ⁻¹]	0.246	0.267	0.212	0.221
Crystal color and shape	colorless plate	colorless plate	colorless plate	colorless block
Crystal size [mm]	0.21 × 0.56 × 0.02	0.23 × 0.55 × 0.05	0.58 × 0.52 × 0.18	0.11 × 0.20 × 0.31
θ range [°]	2.895–27.477	2.902–27.485	2.560–27.485	2.582–27.484
<i>F</i> (000)	292	968	324	684
Reflections				
measured	5060	8584	6170	13,063
unique	3040	2607	3637	7280
Observed data [<i>I</i> > 2 σ (<i>I</i>)]	2382	2252	2317	4470
<i>R</i> _{int}	0.0274	0.0263	0.0324	0.0592
Completeness to θ_{\max}	0.999	0.999	0.999	0.999
Goodness-of-fit on <i>F</i> ²	1.017	1.048	1.034	1.017
<i>R</i> ₁ , <i>wR</i> ₂ [<i>I</i> > 2 σ (<i>I</i>)]	0.0421, 0.0906	0.0313, 0.0752	0.0534, 0.1299	0.0672, 0.1158
<i>R</i> ₁ , <i>wR</i> ₂ (all data)	0.0621, 0.1023	0.0391, 0.0799	0.0893, 0.1528	0.1250, 0.1417
Residual density [e Å ⁻³]	0.289, −0.252	0.264, −0.271	0.305, −0.204	0.345, −0.326
Deposition no	2304064	2304065	2304066	2304067

Table 2. Hydrogen-bond parameters of co-crystals 1–3 and salt solvate 4.

D–H...A *	D–H [Å]	H...A [Å]	D...A [Å]	D–H...A [°]	* Symmetry Code for A
[2-AP·HBTA] (1)					
O2–H1O2...N1	0.96(3)	1.65(3)	2.595(2)	169(3)	<i>x</i> , <i>y</i> + 1, <i>z</i>
N3–H1N3...O1	0.91(2)	2.09(3)	2.978(2)	167(2)	<i>x</i> , <i>y</i> − 1, <i>z</i>
N3–H2N3...N2	0.82(2)	2.27(2)	3.090(3)	176(2)	− <i>x</i> − 1, − <i>y</i> + 1, − <i>z</i> + 1
C13–H13...O2	0.93	2.66	3.531(3)	157.1	− <i>x</i> + 1, − <i>y</i> + 1, − <i>z</i> + 1
[5-AP·2(HBTA)] (2)					
O1–H1O1...N1	0.90(2)	1.74(2)	2.6361(14)	176(2)	<i>x</i> , <i>y</i> − 1, <i>z</i>
N2–H1N2...O2	0.847(16)	2.268(17)	3.0225(16)	148.6(15)	
C10–H10...O2	0.93	2.56	3.2693(17)	133.1	<i>x</i> , <i>y</i> + 1, <i>z</i>
C10–H10...O2	0.93	2.56	3.2693(17)	133.1	− <i>x</i> + 3/2, <i>y</i> + 1, − <i>z</i>
C11–H11...S1	0.93	2.84	3.7208(13)	158.5	
[2-A-4,6-DMP·HBTA] (3)					
O2–H1O2...N1	1.01(3)	1.64(3)	2.645(2)	170(3)	
N3–H1N3...O1	0.81(2)	2.11(3)	2.916(3)	172(2)	
N3–H2N3...N2	0.83(2)	2.20(2)	3.036(3)	177(2)	− <i>x</i> − 1, − <i>y</i> + 2, − <i>z</i> + 1
C3–H3A...O2	0.97	2.54	3.249(3)	129.5	

Table 2. Cont.

D–H...A *	D–H [Å]	H...A [Å]	D...A [Å]	D–H...A [°]	* Symmetry Code for A
[2(2,4,6-TAP⁺)·2(BTA[−])·MeOH] (4)					
N2–H1N2...O4	0.95(3)	1.74(4)	2.684(3)	176(3)	$-x - 1, -y + 1, -z$
N7–H1N7...O2	0.93(4)	1.80(4)	2.724(3)	173(3)	$-x - 1, -y, -z$
N3–H2N3...O2	0.90(3)	2.24(3)	3.028(3)	146(2)	$x - 1, y, z$
N4–H1N4...O3	0.85(4)	1.99(4)	2.842(4)	179(3)	$-x - 1, -y + 1, -z$
N4–H2N4...O1	0.83(3)	2.10(3)	2.906(4)	164(3)	
N5–H2N5...O2	0.94(3)	2.03(4)	2.921(3)	158(3)	$-x, -y, -z + 1$
N8–H1N8...O4	0.89(4)	2.07(4)	2.957(3)	176(3)	$-x - 1, -y + 1, -z$
N8–H2N8...O1	0.95(3)	1.91(3)	2.853(4)	169(3)	$-x - 1, -y, -z$
N9–H2N9...O3	0.85(4)	2.03(4)	2.877(3)	173(4)	$-x - 2, -y + 1, -z$
N3–H1N3...N6	0.82(4)	2.23(4)	2.947(4)	146(3)	
N5–H1N5...N1	0.84(3)	2.41(3)	3.147(4)	146(3)	$-x - 1, -y, -z + 1$
N9–H1N9...N3	0.83(3)	2.48(4)	3.249(4)	155(3)	$-x - 2, -y, -z$
N10–H2N10...O5	0.89(3)	1.98(3)	2.835(4)	161(3)	$x - 1, y, z$
N5–H1N5...S2	0.84(3)	2.91(3)	3.534(3)	133(3)	$-x - 1, -y + 1, -z + 1$
O5–H1O5...S1	0.75(5)	2.56(5)	3.297(3)	165(4)	
C12–H12...S1	0.93	2.81	3.646(3)	150.5	

2.3. Instrumentation and Measurement Methodology

A Perkin Elmer 2400 Series II CHNS/O elemental analyzer (PerkinElmer Inc., Waltham, MA, USA) operating with the CHNS mode was employed to determine the percentage contents of carbon, hydrogen, nitrogen, and sulfur in adducts 1–4.

A SETSYS 16/18 (Setaram, Caluire, France) thermal apparatus registering the TG and DSC thermal curves was used to measure the thermal behavior of complexes 1–4, as well as the thermal properties of individual molecular components. Weighted samples (7.085–8.692 mg) were placed in the alumina crucibles and scanned from 30 to 800 °C. The TG/DSC measurements were conducted under the dynamic air atmosphere (at a rate of airflow of 0.75 dm³ h^{−1}) with a constant heating rate of 10 °C min^{−1}.

An FT/IR-4600 (JASCO Corporation, Tokyo, Japan) Fourier-transform infrared spectrometer was utilized to receive the transmission infrared spectra of all the starting molecular ingredients and co-crystallization products. The spectra of the tested compounds in the region of 4000–400 cm^{−1} were recorded as pressed disks in the KBr matrix.

3. Results and Discussion

The four novel supramolecular organic frameworks based on HBTA and selected aminopyrimidines as co-formers (Figure 1) were profitably received in the form of good X-ray-quality single crystals. The well-shaped single crystals of multi-component molecular materials 1–4 (Figure 3) were grown by utilizing the solution co-crystallization relying on the natural evaporating method according to the synthesis details presented in the Materials and Methods section. The prepared SOFs (Figure 3) are characterized by different stoichiometry despite the inclusion of the same molar ratio of starting molecular entities in co-crystallization. Only in the case of adduct 4 formed from HBTA and 2,4,6-TAP was one MeOH solvent molecule incorporated into the crystal lattice. The co-crystallization products were also investigated by employing FT-IR spectroscopy and thermal analysis in the air to support the results gained from the SC XRD structural study.

3.1. Structural and Supramolecular Characteristics

The aminopyrimidine-based supramolecular complexes 1–4 were defined as [2-AP·HBTA] (1), [5-AP·2(HBTA)] (2), [2-A-4,6-DMP·HBTA] (3), and [2(2,4,6-TAP⁺)·2(BTA[−])·MeOH] (4). The disclosed compositions of the residues present in the crystal lattices indicate that the isolated crystals belong to two different forms, distinguished by the classification procedure of

multicomponent crystalline phases [10], that is, co-crystal (architectures 1–3) and salt solvate (adduct 4).

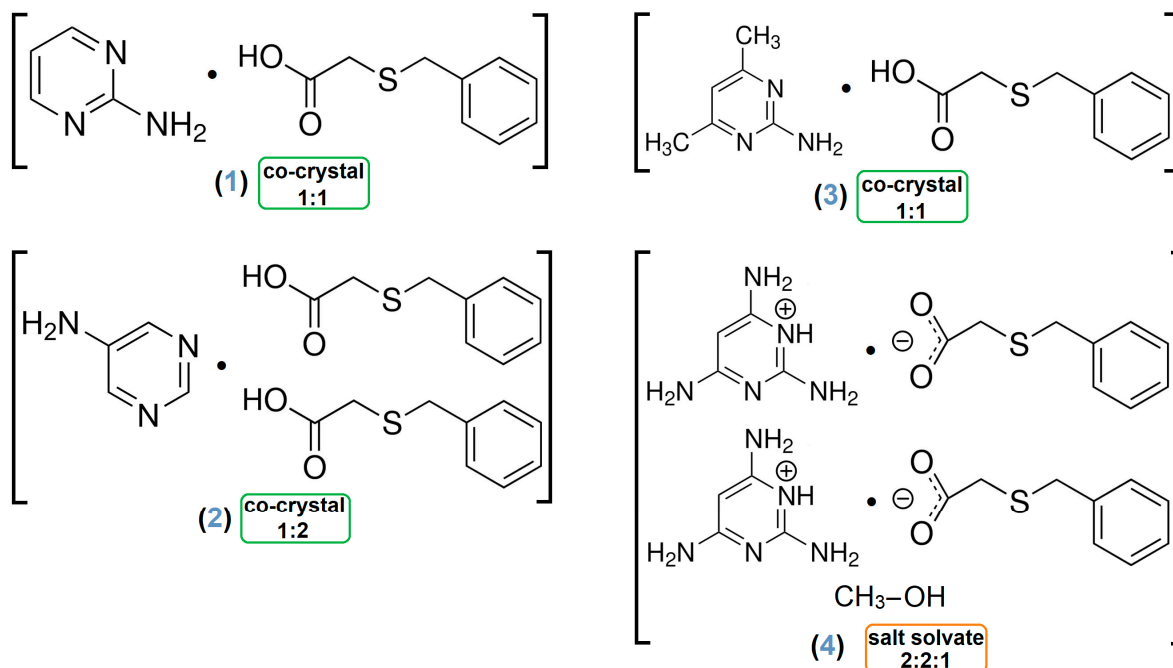


Figure 3. The chemical diagrams of adducts 1–4.

3.1.1. Co-Crystal Obtained from 2-AP and HBTA (1)

Compound 1 crystallizes in the triclinic crystal system in the *P*-1 space group (Table 1). The atom numbering and the conformation of 1 in the crystal are shown in Figure 4. The asymmetric unit of 1 consists of one HBTA and one 2-AP molecule. The C1–O1 and C1–O2 bond lengths of the acid molecule are equal to 1.217(3) Å and 1.309(3) Å, respectively, indicating that the hydrogen atom is located on the O2 atom (Figure 4A). The pyrimidine ring lies almost in the same plane as the alkyl chain of the acid molecule, whereas the dihedral angle between the plane of the phenyl ring of the HBTA molecule and the pyrimidine moiety of 2-AP is 116.2° (Figure 4B).

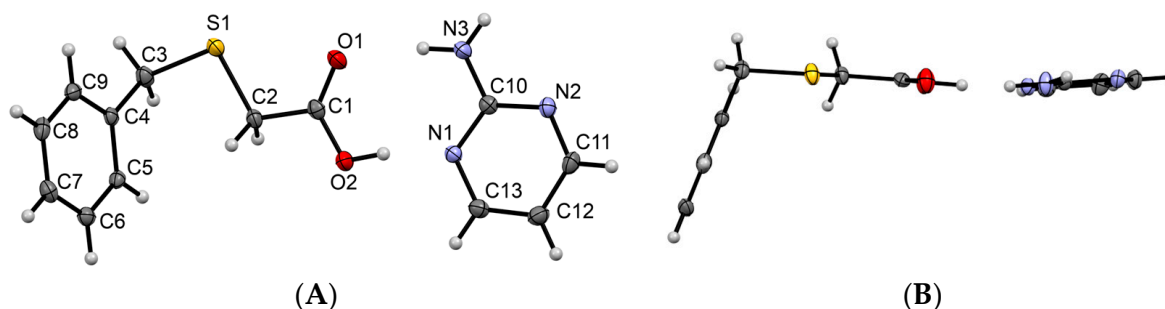


Figure 4. Representation of the asymmetric unit of 1 with the atom labeling scheme (A) and the orientation of the phenyl ring of the acid molecule with respect to pyrimidine moiety (B). Displacement ellipsoids are drawn at 50% probability level.

The primary hydrogen bonding observed in the [2-AP·HBTA] co-crystal is an aminopyrimidine···acid dimer (Figure 5). This $R_2^2(8)$ heterodimer is formed by O2–H···N1 and N3–H···O1 hydrogen bonds (Donor···Acceptor distances and D–H···A angles are given in Table 2). Such hydrogen-bonding geometry, comprising the carboxylic/carboxylate O atoms associated with the heterocyclic N atom and the 2-amino group, is characteristic of co-crystals [20,41] and salts [2,16] of 2-aminopyrimidine with

aromatic carboxylic acids. Such dimers in [2-AP·HBTA] are connected alternately by two synthons: the N3–H···N2 hydrogen bond and the C13–H···O2 interaction (Figure 5). Both synthons partake in the formation of two further ring motifs: homomeric ring $R_2^2(8)$ formed by the N3–H···N2 bond and a tetramer based upon a centrosymmetric $R_4^4(10)$ motif based on C13–H···O2 contact and the O2–H···N1 hydrogen bond. All these synthons take part in the formation of a stable ribbon, as presented in Figure 5. Such a ribbon is a characteristic structural motif for co-crystals containing 2-AP [20].

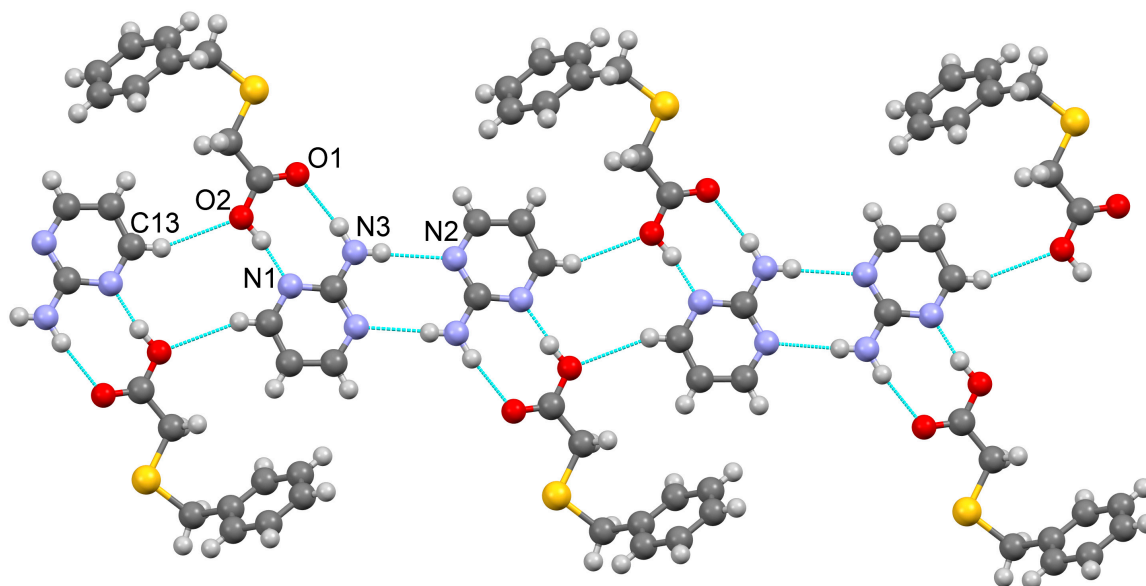


Figure 5. H-bond synthons in the crystal lattice of **1**.

The $C2_{\text{acid}}\text{-H}\cdots\pi_{\text{pyrimidine}}$ contacts and $\pi\cdots\pi$ interactions between the 2-AP molecules link the ribbons into a three-dimensional structure (Figure 6), which is additionally stabilized by the weak intermolecular C–H···O bonds formed between two acid molecules as well as between acid and 2-AP molecules.

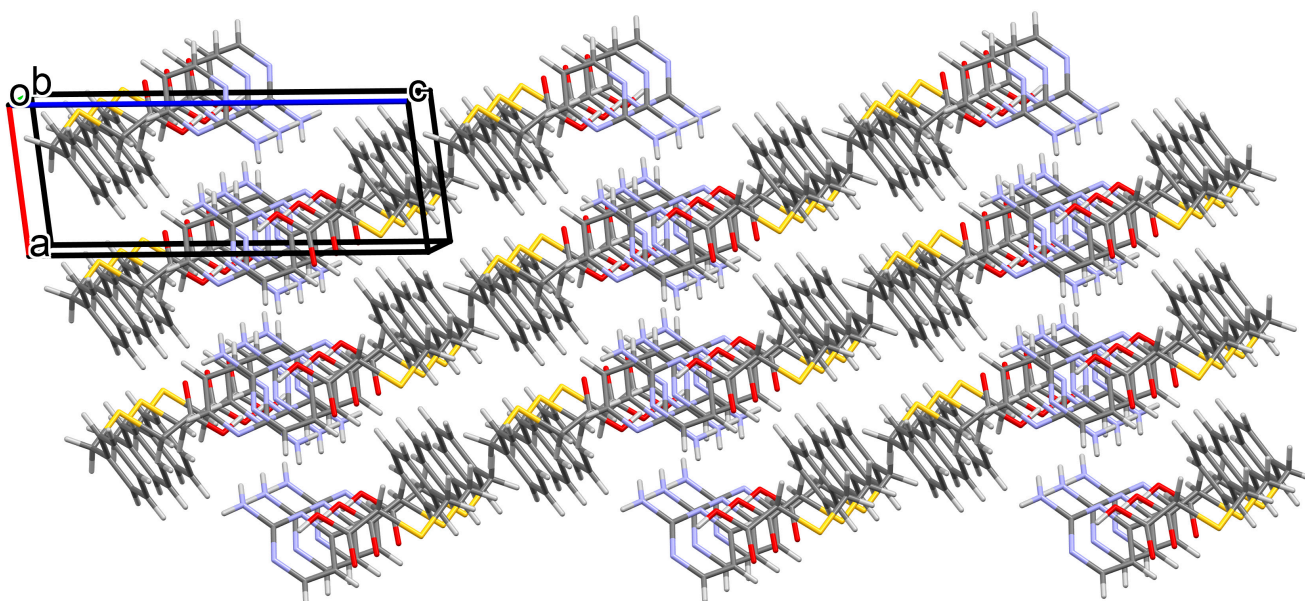


Figure 6. Crystal-packing diagram of **1** along *b*-axis.

3.1.2. Co-Crystal Formed between 5-AP and HBTA (2)

Compound **2** crystallizes in the monoclinic $I2/a$ space group (Table 1) with one molecule of HBTA and half a molecule of 5-AP in the asymmetric unit. The C1–O1 bond length is equal to 1.322(2) Å, being longer than the C1–O2 bond (1.210(2) Å), which proves the localization of the hydrogen atom on the O1 atom of the acid molecule (Figure 7A). The conformation of the alkyl sulfanyl chain of the HBTA molecule in the co-crystal with 5-AP (**2**) differs from its planar architecture in the co-crystal with 2-AP (**1**) (Figures 4B and 7B). The torsional angle C3–S1–C2–C1 is equal to $-68.8(1)^\circ$ for compound **2**, whereas for compound **1**, it was $-179.1(1)^\circ$. The pyrimidine moiety of compound **2** lies almost in the same plane as the S1–C2–C1 chain of the acid molecule, and the dihedral angle between the planes of the phenyl and pyrimidine rings is 46.1° .

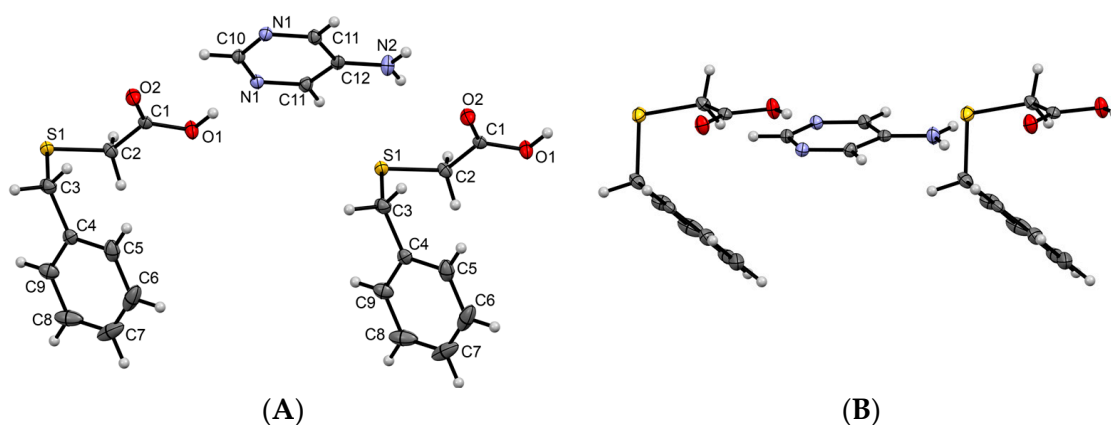


Figure 7. The molecular structure of **2** with the atom-numbering scheme (A) and the orientation of the phenyl ring of the acid molecule with respect to pyrimidine moiety (B). Displacement ellipsoids are drawn at 50% probability level.

The molecule of HBTA is bonded to two 5-AP molecules resulting in the formation of two types of dimers: $R_2^2(9)$ and $R_2^2(8)$ (Figure 8). The $R_2^2(9)$ dimer is formed by N2–H \cdots O2 and C11–H \cdots S1 contacts (Table 2), and the 5-AP molecule acts as a donor and the HBTA molecule becomes hydrogen bond acceptor. The second dimer, described with the $R_2^2(8)$ graph-set motif, is formed through O1–H \cdots N1 and C10–H \cdots O2 interactions. In this dimer, both components act as hydrogen bond donors and acceptors. Both dimers, repeated with a two-fold axis passing through the pyrimidine rings, form a tetramer.

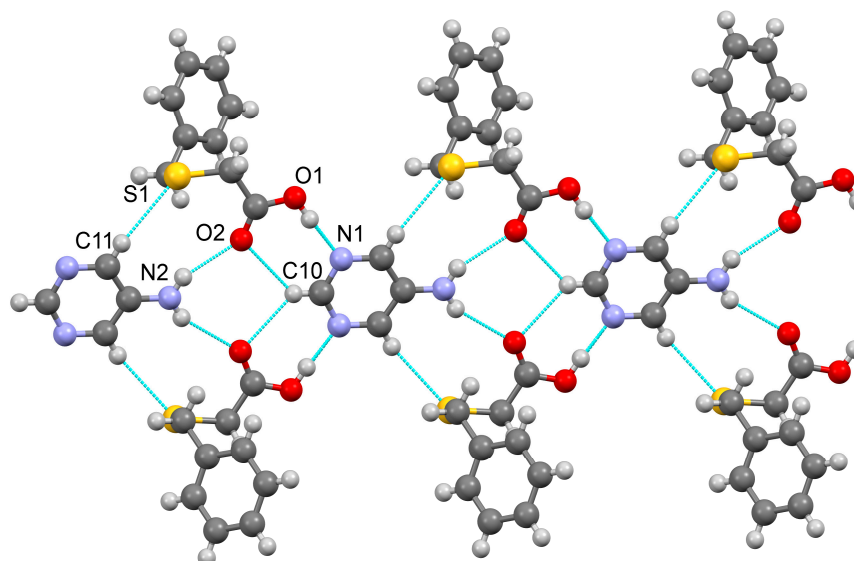


Figure 8. H-bond synthons in the crystal lattice of **2**.

The 5-AP molecules link such tetramers in a strong ribbon-like structure (Figure 8) that is further stabilized by the C8–H···O1, C10–H···O2, and C2–H···N2 contacts, as well as C–H··· π interactions between HBTA molecules, forming a 3D supramolecular architecture of co-crystal 2 (Figure 9). Comparing the hydrogen-bond interactions within the 3D network of 5-AP and 2-AP with HBTA, we see that for both co-crystals, one of the hydrogen bonds is significantly stronger than the others. While for most interactions, the donor···acceptor distance is equal to or greater than 3 Å, in the case of the O–H···N synthon, it is equal to 2.6361(14) Å for co-crystal 2 and 2.595(2) Å for co-crystal 1 (Table 2). Such short O–H···N hydrogen bond distances between the hydroxyl group of carboxylic acid and the N-atom of the pyrimidine moiety are observed for analogous compounds [20,41] and indicate that the O–H···N interaction plays a key role in the structure stabilization of the co-crystals in question.

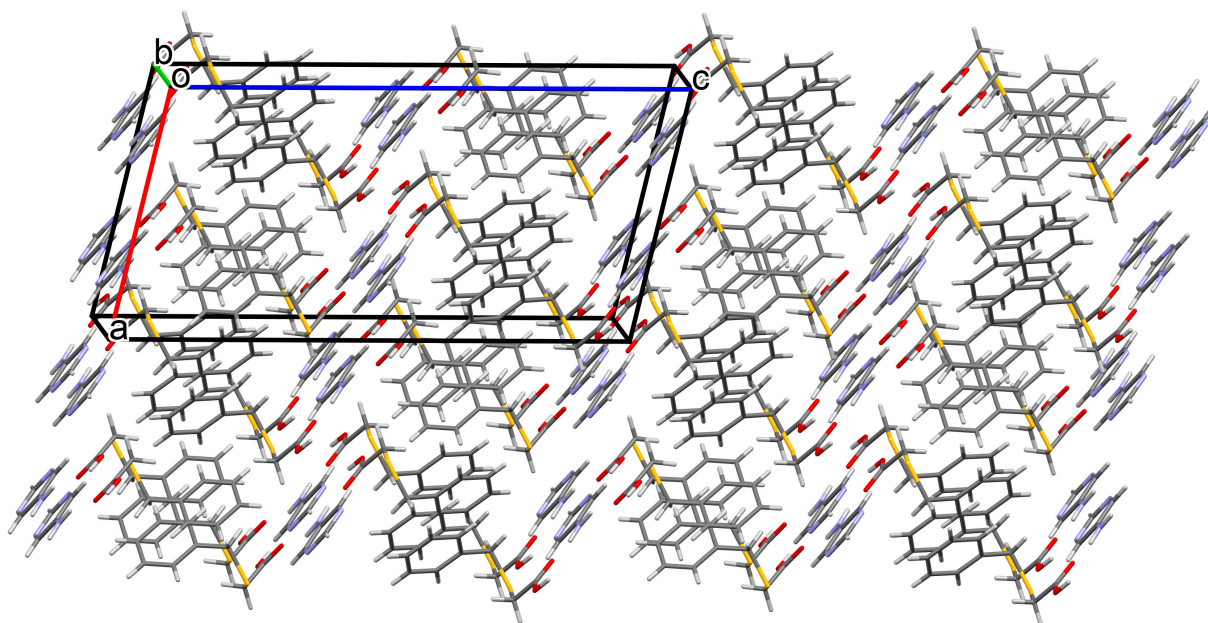


Figure 9. Crystal-packing diagram of 2 along *b*-axis.

3.1.3. Co-Crystal Based on 2-A-4,6-DMP and HBTA (3)

The crystal structure analysis of 3 reveals a 1:1 co-crystal that crystallizes in the triclinic *P*-1 space group (Table 1). The asymmetric part of 3 consists of one neutral molecule of HBTA and one neutral molecule of 2-A-4,6-DMP. The length of the C1–O1 and C1–O2 bonds are 1.211(2) Å and 1.303(3) Å, respectively, indicating that the H atom is located on the O2 atom of the acid molecule (Figure 10A). The torsional angle C3–S1–C2–C1 in HBTA is $-84.9(2)^\circ$. Such stereochemistry of the alkyl sulfanyl chain of acid molecule causes the formation of the C3–H···O2 intramolecular hydrogen bond. The phenyl part of HBTA and the pyrimidine ring are approximately perpendicular to each other (Figure 10B), and the value of the dihedral angle between the planes formed by these moieties is 76.5° .

The carboxyl group of HBTA and the 2-A-4,6-DMP molecule act as donors and acceptors of the hydrogen bond, forming the $R_2^2(8)$ heterodimer through O2–H···N1 and N3–H···O1 contact (Figure 11, Table 2). Such a synthon is similar to the dimer motif observed in co-crystal 1, which is related to the presence of the $-NH_2$ group at C10 of the pyrimidine ring. Two 2-A-4,6-DMP molecules in co-crystal 3 are linked via the N3–H···N2 hydrogen bonds, and the formation of the centrosymmetric homomeric $R_2^2(8)$ dimer is observed. All described synthons build a tetrameric supramolecular unit as presented in Figure 11. Such a linear heterotetramer motif is observed in analogous co-crystals and salts of 2-amino-4,6-dimethoxypyrimidine as well as 4,6-dimethylpyrimidine with carboxylic acids [1]. Both methyl and methoxy groups in positions 4 and 6 of the pyrimidine ring

prevent the formation of a larger number of strong intermolecular interactions and the three-dimensional structure is created through the weaker hydrogen bonds.

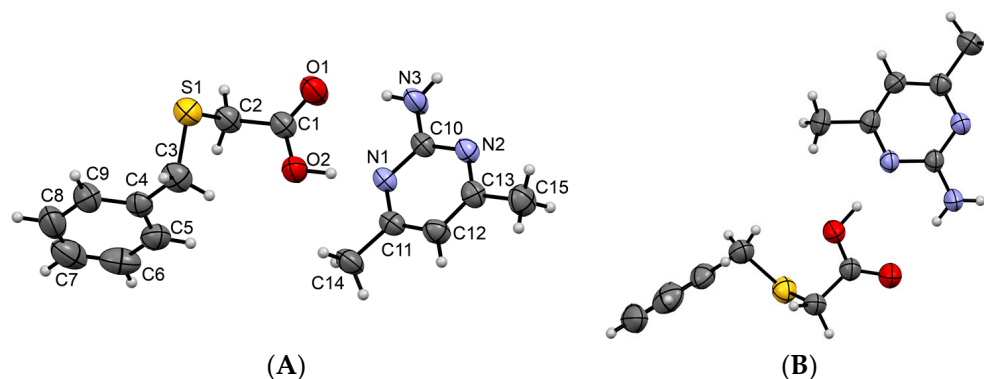


Figure 10. Representation of the asymmetric unit of **3** with the atom-labeling scheme (A) and the orientation of the phenyl ring of the acid molecule with respect to pyrimidine moiety (B). Displacement ellipsoids are drawn at 50% probability level.

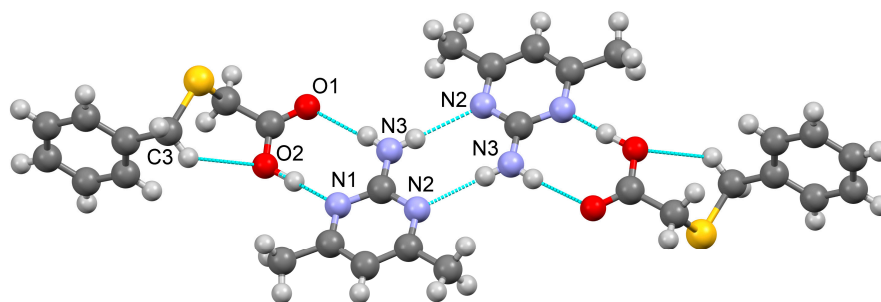


Figure 11. H-bond synthons in the crystal lattice of **3**.

In [2-A-4,6-DMP·HBTA], tetrameric units are connected via C2–H··· π (HBTA···HBTA) and C12–H··· π (2-A-4,6-DMP···HBTA) contacts, forming a 2D layer. The C9–H···S1 and C6–H···O1 interaction between the acid molecules expands the layer into a stable 3D hydrogen-bonded network, as presented in Figure 12.

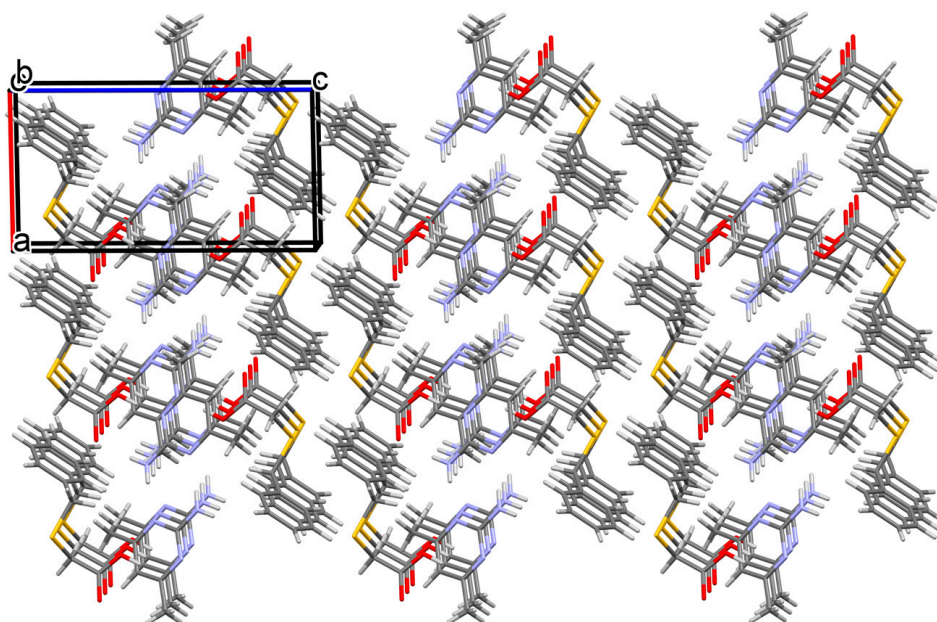


Figure 12. Crystal-packing diagram of **3** along *b*-axis.

3.1.4. Salt Methanol Solvate Derived from 2,4,6-TAP and HBTA (4)

Compound 4 crystallizes in the triclinic $P-1$ space group (Table 1). The 2,4,6-TAP forms a 2:2:1 molecular adduct with HBTA and the solvent. However, proton transfer occurs by generating a salt, not a co-crystal as in the case of the compounds containing the monoaminopyrimidine component (compounds 1–3). The asymmetric unit of 4 consists of two BTA^- anions, two $2,4,6\text{-TAP}^+$ cations, and one MeOH molecule (Figure 13). The bond lengths C1–O1/O2 and C14–O3/O4 are equal to 1.240(4)/1.277(5) Å and 1.246(4)/1.269(5) Å, respectively, which confirms the deprotonation of acid molecules. The stereochemistry of alkyl chains differs between two acid anions—the torsional angles of C3–S1–C2–C1/C16–S2–C15–C14 are 174.9(3)/78.7(3)°.

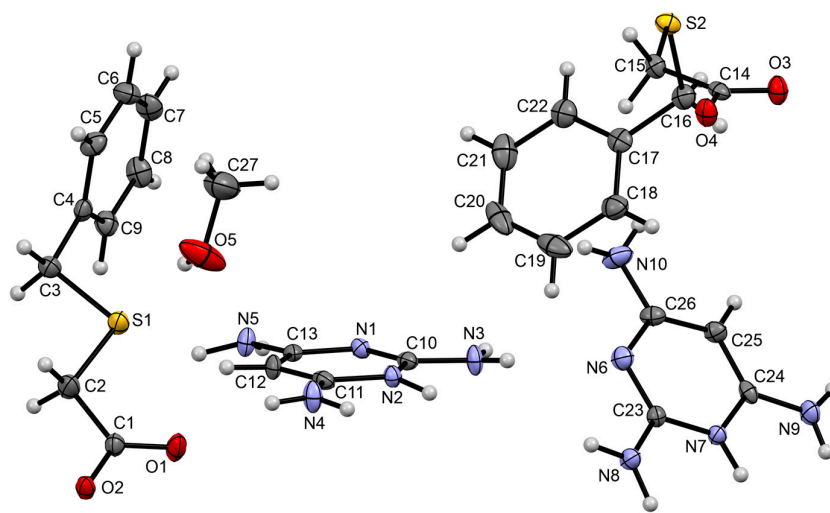


Figure 13. The asymmetric unit of 4 with the atom-numbering scheme. Displacement ellipsoids are drawn at 50% probability level.

The crystal structure analysis of 4 revealed the presence of as many as 10 types of N–H···O, three types of N–H···N, and one type of N/O–C–H···S synthons, presented in detail in Table 2. Such a complex hydrogen-bonding scheme, arising from the superabundance of donors and acceptors, leads to the formation of a stable 3-D structure, as presented in Figure 14.

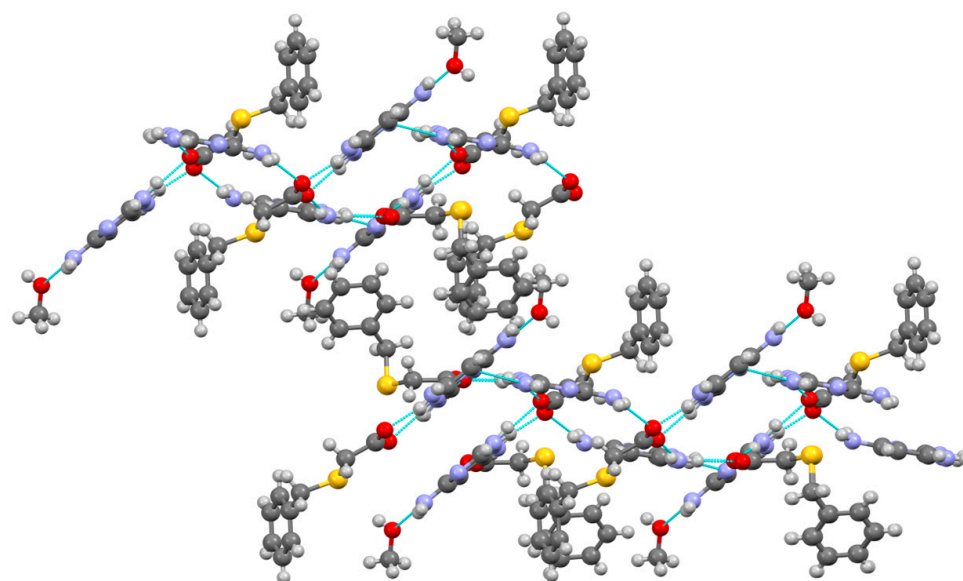


Figure 14. H-bond synthons in the crystal lattice of 4.

Analyzing the geometries of the N–H···O hydrogen bonds dominating in this structure, we see that the donor···acceptor distances are in the wide range from 2.684(3) to 3.028(3) Å and are significantly shortened compared to those observed in co-crystals 1–3 (Table 2). Shortening the bond length is due to hydrogen proton transfer between the adjacent components, and the same phenomenon is observed with other salts of 2,4,6-TAP [29,32]. Additionally, C6–H···O3 (BTA[−]···BTA[−]) and O5–H···S1 (MeOH···BTA[−]) contacts become important in the stabilization of the 3-D structure of salt 4 (Figure 15).

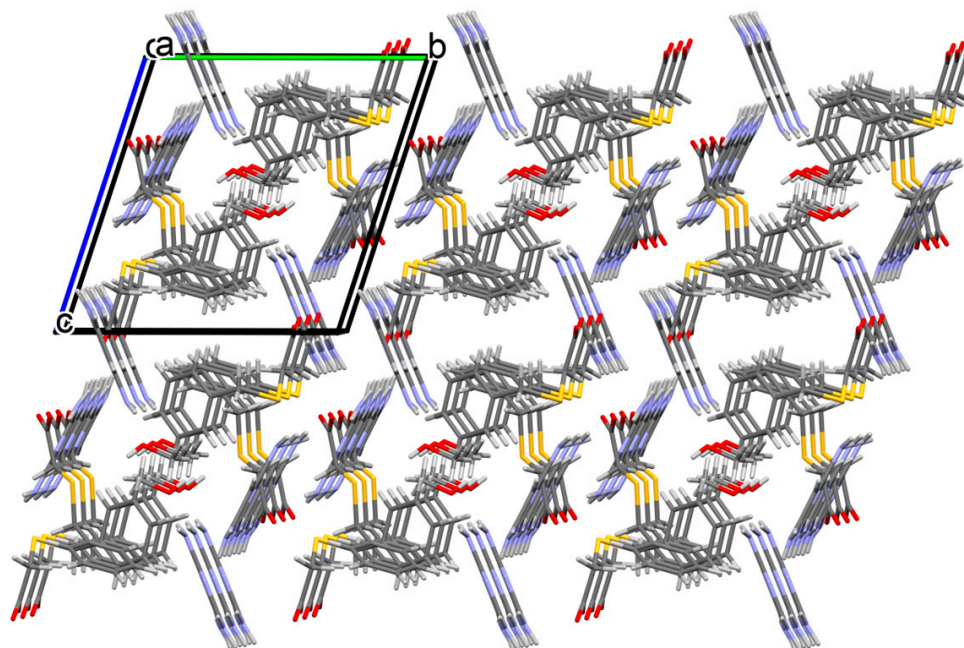


Figure 15. Crystal-packing diagram of 4 along *a*-axis.

3.2. Thermal Behavior in the Air Atmosphere

The novel crystalline solids were investigated through thermal analysis based on thermogravimetry (TG) combined with differential scanning calorimetry (DSC) in order to establish their composition and thermal behavior under controllable heating. The summary of the TG and DSC courses for supramolecular complexes 1–4 against the TG and DSC traces of corresponding molecular components are presented in Figures 16 and 17, respectively. Additionally, the separate illustrations presenting the thermograms for individual complexes and their starting components are given in Supplementary Material as Figures S1–S4, respectively. As follows from Figures 16 and 17, all supramolecular materials are characterized by different courses of their thermal traces in relation to the thermal curves for starting co-partners, which clearly indicate the formation of novel multi-component crystalline phases.

The supramolecular complexes 1–3 are unsolvated solids that are thermally stable up to approximately 108 °C, 109 °C, and 135 °C, respectively, as indicated by the plateau visible on their TG profiles in the above temperature ranges. Complex 4 is stable at room temperature and was defined as a monosolvate. In the case of conglomerate 4, the desolvation process takes place in one stage above 40 °C. The removal of the MeOH molecule corresponding to the first weight loss of 5.16% was found on the TG plot up to 132 °C, which coincided with the theoretical value of 4.95%. The release of the MeOH molecule is also echoed with the first detectable endothermic effect seen on the DSC curve with the peak top located at 83 °C, indicating the lower stability for the heat of the salt solvate against co-crystals. The higher temperature of MeOH liberation exhibited by complex 4 compared to the boiling point of pure MeOH suggests the interaction of methanol molecules with co-partner residues through intermolecular H-bonds. After the loss of the MeOH molecule, the unstable product in the form of the unsolvated

salt begins to decompose immediately up to 750 °C along with the burning of cationic and anionic residues in two evident steps. Each of the two stages of combustion of the ions is associated with an identical mass loss (found: 47.42%; calcd.: 47.52%), which indicates that in each decomposition stage, one TAP⁺ and one BTA⁻ residue from the asymmetric unit is burned. The first stage of exothermic decomposition, proceeding between 132 °C and 330 °C, is connected only to the combustion of those TAP⁺ and BTA⁻ species that formed H-bonds with MeOH, whereas the second exothermic degradation step, going from 132 °C to 750 °C, is associated with the burning of those ionic residues that were not H-bonded to the solvent, which is consistent with the crystal structure of salt solvate 4. Further heating above the level of thermal resistance of co-crystals 1–3 causes the explosion of all base and acidic components up to approximately 538 °C, 648 °C, and 570 °C, respectively, reflected by several exothermic peaks situated on their DSC traces. The strongest heat releases during the decomposition process are visible on DSC profiles as the most intense exothermic maxima located near 477 °C (1) (Figure S1), 526 °C (2) (Figure S2), 503 °C (3) (Figure S3), and 668 °C (4) (Figure S4). The characteristically sharp and single peak seen in each DSC thermogram reflects the endothermic effect of the melting process of a given compound. The unsolvated forms of adducts, namely [2-AP·HBTA] (1), [5-AP·2(HBTA)] (2), [2-A-4,6-DMP·HBTA] (3), and [2(2,4,6-TAP⁺)·2(BTA⁻)] (4), melt before the exothermic degradations of co-partner residues. The melting points of associations 1–4 have distinct values (87 °C (1), 96 °C (2), 105 °C (3), and 125 °C (4)) compared to the melting points of the starting ingredients (64 °C (HBTA) [34], 127 °C (2-AP) [13], 173 °C (5-AP), 153 °C (2-A-4,6-DMP) [21], and 248 °C (2,4,6-TAP)), which clearly proves the formation of novel crystalline solids without phase impurity. The melting points of adducts 1–4 lie between the melting points of the corresponding co-partners, which is typical for binary crystals. Finally, all crystals decompose with approximately 100% sample weights converted into gaseous decomposition products.

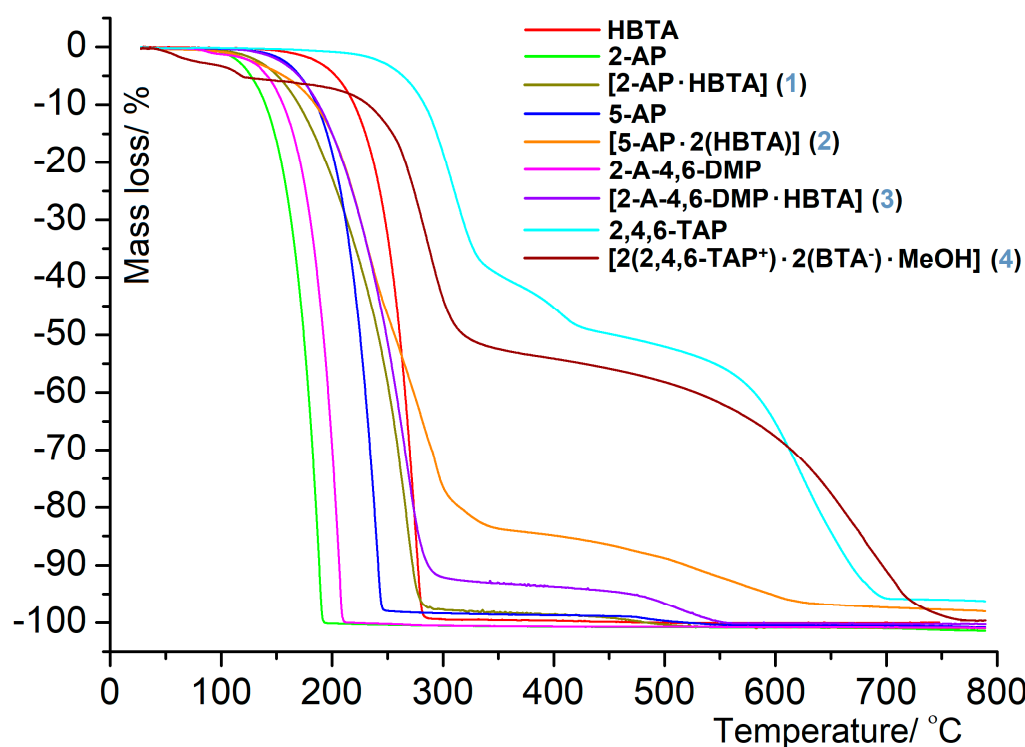


Figure 16. The TG profiles of supramolecular adducts 1–4 along with the TG curves of suitable molecular building bricks between 30 and 800 °C.

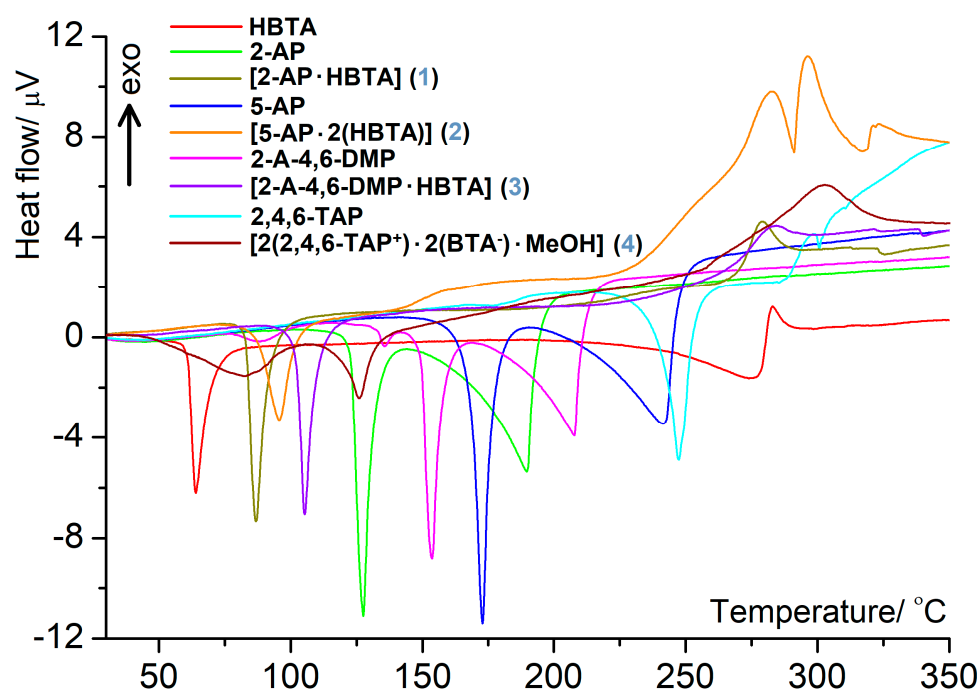


Figure 17. The DSC curves of supramolecular assemblies 1–4 in comparison to DSC plots of the molecular components between 30 and 350 °C.

3.3. FT-IR Characteristics

FT-IR spectroscopy is a significant technique for characterizing crystalline solids in terms of distinguishing co-crystals or salts, especially when one of the co-partners is a carboxylic derivative. The determination of multi-component crystalline phases in the co-crystal/salt category is based on the identification of functional groups within the molecular co-partners embodied in the supramolecular complexation process. The FT-IR spectra of starting ingredients and their ground mixtures are illustrated in Figures 18 and 19. The spectral traces recorded for phases 1–4 show that both the acidic and suitable basic residues are present in the tested solids, but the supramolecular complexation between them through intermolecular contacts resulted in shifting of characteristic stretching vibrational modes derived from the starting co-partners. The formation of these new multi-component solid forms is especially displayed by shifting of stretching vibrations of those functionals, like $-\text{COOH}$, $-\text{NH}_2$, and the N -pyrimidine atom, which are the strong sites in H-bonding.

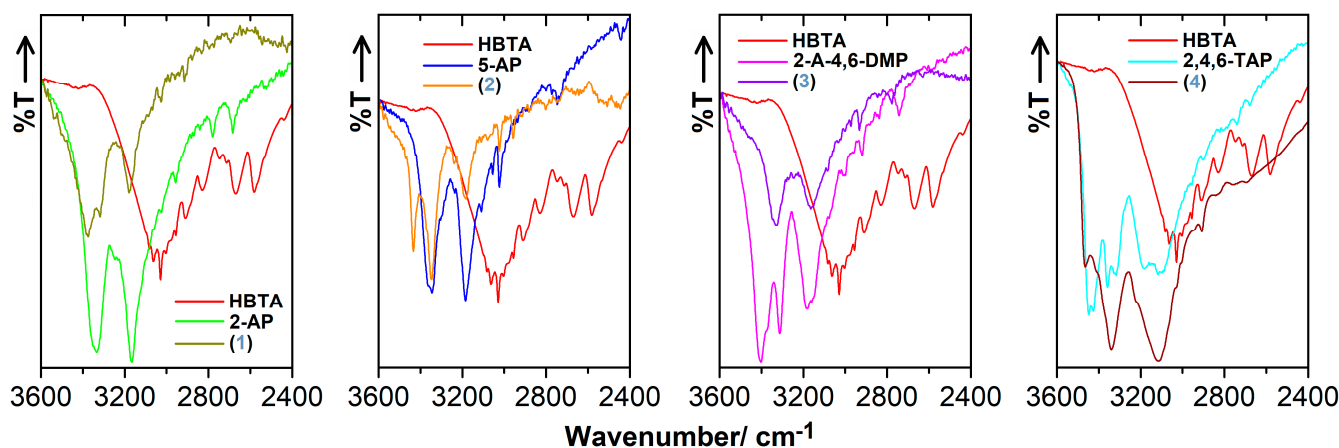


Figure 18. The comparison of infrared spectral traces in the range of 3600–2400 cm^{-1} for associations 1–4 as well as the free co-partners.

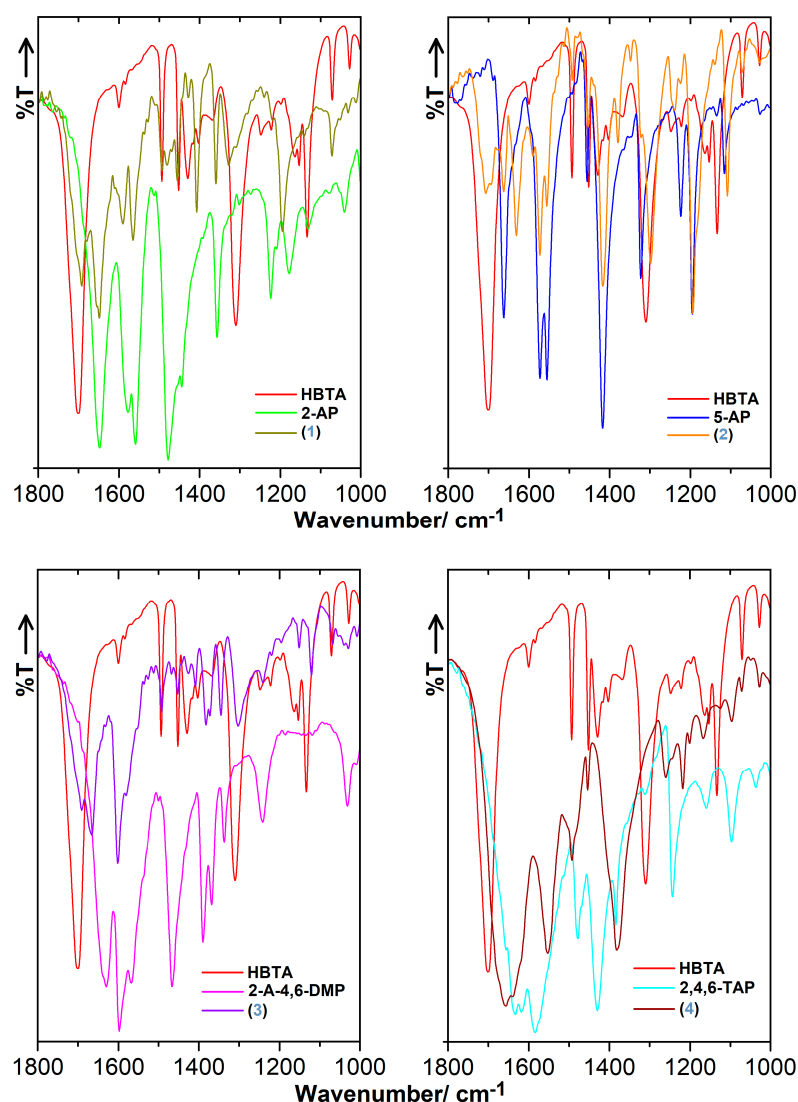


Figure 19. The FT-IR profiles for phases 1–4 in relation to the infrared plots of starting components in the region of 1800 and 1000 cm^{-1} .

The HBTA molecule possesses one neutral acidic $-\text{COOH}$ motif. The HBTA spectrum recorded in the KBr matrix is dominated by the strongest absorption band at 1697 cm^{-1} [42] associated with the stretching $\nu(\text{C}=\text{O})$ vibrational mode of the carbonyl part of the $-\text{COOH}$ group. The spectral profiles of associations 1–3 (Figure 19) bear the most diagnostic vibrational mode of acidic functional, but its position is slightly shifted in relation to its location in the spectrum of free HBTA ingredients. The bands of stretching $\nu(\text{C}=\text{O})$ vibrations are observed for adducts 1–3 at 1692 cm^{-1} (1), 1707 cm^{-1} (2), and 1691 cm^{-1} (3), respectively. The presence of the absorption peaks corresponding to the $\nu(\text{C}=\text{O})$ stretches is the most reliable proof concerning the co-crystal formation, coinciding with the SC X-ray data regarding the lack of proton transfer from the acidic co-partner to the base during supramolecular complexation. On the other hand, the basic co-partners in the form of 2-AP, 5-AP, and 2-A-4,6-DMP have only one $-\text{NH}_2$ group, which is identified by the high-energy absorption bands of asymmetric $\nu_{as}(\text{NH}_2)$ and symmetric $\nu_s(\text{NH}_2)$ stretching vibrations situated at 3334 cm^{-1} and 3165 cm^{-1} (3330 cm^{-1} and 3150 cm^{-1} [43]) for 2-AP, 3345 cm^{-1} and 3184 cm^{-1} for 5-AP, and 3314 cm^{-1} and 3182 cm^{-1} (3311 and 3168 cm^{-1} [44]) for 2-A-4,6-DMP. Moreover, the spectrum of 2-A-4,6-DMP contains a strong and broadened absorption band comprising the maximum at 3402 cm^{-1} and the shoulder at 3379 cm^{-1} , which is absent after complexation with HBTA. Besides a single-component crystal [45],

the 2-A-4,6-DMP under ambient conditions may also form a true solvate in the form of a monohydrate [46]. Thus, the aforementioned frequencies are actually associated with the asymmetric and symmetric combination of stretching $\nu(\text{OH})$ vibrations originating from the incorporated water molecule. The monohydrate nature of 2-A-4,6-DMP used as a co-partner in this study is also indicated in the TG and DSC thermal results (Figures 16, 17 and S3). The visible mass loss of 1.32% (calcd.: 1.44%) seen on the TG plot up to 106 °C supported by the endothermic effect visible on the DSC curve at 88 °C clearly points to the monohydrated nature of 2-A-4,6-DMP. The $\nu_{as}(\text{NH}_2)$ and $\nu_s(\text{NH}_2)$ stretch of the amino group derived from the suitable aminopyrimidine component in the registered spectra of complexes 1–3 is active at 3376 cm^{-1} and 3180 cm^{-1} (1), 3346 cm^{-1} and 3181 cm^{-1} (2), and 3331 cm^{-1} and 3164 cm^{-1} (3), respectively. The spectral data concerning the $\nu_{as}(\text{NH}_2)$ and $\nu_s(\text{NH}_2)$ fundamentals found in the spectra of conglomerates 1–3 indicate that the basic ingredients remain in their original figure and are consistent with the previously published infrared data associated with co-crystals formed between 2-AP and 1,4-cyclohexanedicarboxylic [11] or 3-nitrophthalic [41] acid and between 2-A-4,6-DMP and benzoic [47], indole-3-acetic [27], or butyric-3-acetic [27] acid.

The infrared spectrum of adduct 4 does not show any peak near 1700 cm^{-1} derived from the $\nu(\text{C}=\text{O})$ stretching vibrational mode of the original form of HBTA. Complex 4 bears two specific bands located at 1551 cm^{-1} and 1379 cm^{-1} assigned to the asymmetric $\nu_{as}(\text{COO}^-)$ and symmetric $\nu_s(\text{COO}^-)$ stretches of the carboxylate group, respectively. The presence of carboxylate stretching motions instead of carbonyl stretching vibrations points to the transfer of an acidic proton from HBTA into 2,4,6-TAP, resulting in the formation of organic salt in this case. The occurrence of co-partners only in ionized forms is also reflected in the designated X-ray crystal structure of assembly 4. 2,4,6-TAP contains three $-\text{NH}_2$ groups, so the numerous maxima observed in the spectrum of free 2,4,6-TAP between 3448 cm^{-1} and 3315 cm^{-1} correspond to the asymmetric $\nu_{as}(\text{NH}_2)$ and symmetric $\nu_s(\text{NH}_2)$ stretching vibrations from amino groups (3460–3316 cm^{-1} [48]). According to the crystal structure of salt solvate 4, it is expected that the highly energetic spectral region is represented by the characteristically broadened and simultaneously overlapping bands associated with the various stretching vibrational modes ($\nu_{as}(\text{NH}_2)$ and $\nu_s(\text{NH}_2)$, $\nu(^+\text{NH})$ and $\nu(\text{OH})$) originating from those functional groups that act as strong H-bonded sites, such as the amino functionals, the pyrimidinium unit, and the hydroxyl group of methanol, respectively.

4. Conclusions

Four novel aminopyrimidine-based multi-component crystalline solids distinguished by phase purity were prepared with HBTA as an acidic ingredient. The generated supramolecular assemblies with binary and tri-component conglomerates were characterized using SC XRD, FT-IR, and TG-DSC techniques. The organic binary adducts obtained from 2-AP, 5-AP, and 2-A-4,6-DMP form co-crystals, whereas the tri-component assembly fabricated with the help of 2,4,6-TAP gives the salt methanol solvate.

It is shown that aminopyrimidines are great supramolecular moieties that generate crystals with different hydrogen bonding networks. Because of the presence of *N*-atoms, all multi-component crystals contain a strong $\text{N}-\text{H}\cdots\text{O}$ interaction: one type observed in three new co-crystals and ten types formed within the crystal structure of the salt methanol solvate. This significant difference in the number of hydrogen bonds is related to the transfer of a proton between the acid molecule and 2,4,6-TAP. When the hydrogen proton is transferred between the adjacent components, it is easier to generate hydrogen bonds at the site of the proton transfer. Neutral molecules in co-crystals with 2-AP, 5-AP, and 2-A-4,6-DMP are connected mainly to one type of $\text{O}-\text{H}\cdots\text{N}$, $\text{N}-\text{H}\cdots\text{O}/\text{N}$, $\text{C}-\text{H}\cdots\text{O}/\text{S}$ hydrogen bond, forming 1D ribbons or tetrameric units. Sixteen types of interactions ($\text{N}-\text{H}\cdots\text{O}/\text{N}/\text{S}$, $\text{O}/\text{C}-\text{H}\cdots\text{S}$) observed in the crystal structure of salt solvate with 2,4,6-TAP cause the creation of a stable 3-D structure. While the salt structure is stabilized by a series of $\text{N}-\text{H}\cdots\text{O}$ hydrogen bonds, the main role in the stabilization of co-crystals is

played by the strong O–H···N synthon, for which the donor···acceptor distance is in the order of 2.6 Å.

On the other hand, the HBTA as a flexible structural fragment efficiently creates the diversiform of supramolecular frameworks with stable H-bonded motifs, which makes it a noteworthy molecular ingredient with high activity for co-crystal/salt formation.

Supplementary Materials: The following supporting information can be downloaded at: <https://www.mdpi.com/article/10.3390/cryst13121628/s1>, Figure S1: TG and DSC traces for HBTA, 2-AP and [2-AP·HBTA] (1) between 30 and 800 °C; Figure S2: TG and DSC plots for HBTA, 5-AP, and [5-AP·2(HBTA)] (2) between 30 and 800 °C; Figure S3: TG and DSC curves for [2-A-4,6-DMP·HBTA] (3) between 30 and 800 °C title; Figure S4: TG and DSC profiles for HBTA, 2-4,6-TAP, and [2(2,4,6-TAP⁺)·2(BTA⁻)·MeOH] (4) between 30 and 800 °C.

Author Contributions: Conceptualization, J.S.-G.; methodology, J.S.-G.; investigation, J.S.-G.; data interpretation, J.S.-G. and A.D.-A.; writing—original draft preparation, J.S.-G. and A.D.-A.; writing—review and editing, J.S.-G. and A.D.-A.; visualization, J.S.-G. and A.D.-A.; supervision, J.S.-G.; project administration, J.S.-G.; funding acquisition, J.S.-G. All authors have read and agreed to the published version of the manuscript.

Funding: This research was financially supported by the National Science Centre (NCN) of Poland within grant number 2019/03/X/ST5/01502.

Institutional Review Board Statement: Not applicable.

Informed Consent Statement: Not applicable.

Conflicts of Interest: The authors declare no conflict of interest.

References

1. Ebenezer, S.; Muthiah, P.T. Design of co-crystals/salts of aminopyrimidines and carboxylic acids through recurrently occurring synthons. *Cryst. Growth Des.* **2012**, *12*, 3766–3785. [[CrossRef](#)]
2. Oruganti, M.; Nechipadappu, S.K.; Khade, P.A.; Trivedi, D.R. Solid-state versatility of the molecular salts/cocrystals of 2-chloro-4-nitrobenzoic acid: A case study on halogen bonds. *ACS Omega* **2017**, *2*, 7146–7162. [[CrossRef](#)] [[PubMed](#)]
3. Mirzaei, M.; Sadeghi, F.; Molčanov, K.; Zareba, J.K.; Gomila, R.M. Recurrent supramolecular motifs in a series of acid–base adducts based on pyridine-2,5-dicarboxylic acid *N*-oxide and organic bases: Inter- and intramolecular hydrogen bonding. *Cryst. Growth Des.* **2020**, *20*, 1738–1751. [[CrossRef](#)]
4. Odiase, I.; Nicholson, C.E.; Ahmad, R.; Cooper, J.; Yufit, D.S.; Cooper, S.J. Three cocrystals and a cocrystal salt of pyrimidin-2-amine and glutaric acid. *Acta Crystallogr.* **2015**, *C71*, 276–283. [[CrossRef](#)] [[PubMed](#)]
5. Zhang, L.; Zhou, J.; Wu, Y.; Wang, P.; Jin, S.; Lu, Y. Noncovalent-bonded 2D-3D supramolecular adducts from 6-methylpyridine-3-carboxamide and carboxylic acids. *J. Mol. Struct.* **2022**, *1264*, 133256. [[CrossRef](#)]
6. Wu, R.; Yu, Y.; Guo, M.; Jin, S.; Wang, D. Eight salts of 4-dimethylaminopyridine and organic acids by H-bonds and some noncovalent associations. *J. Mol. Struct.* **2021**, *1230*, 129850. [[CrossRef](#)]
7. Xu, W.; Hu, K.; Lu, Y.; Ye, H.; Jin, S.; Li, M.; Guo, M.; Wang, D. The crystal structures of ten supramolecular salts of benzylamine and organic acids. *J. Mol. Struct.* **2020**, *1219*, 128554. [[CrossRef](#)]
8. Groom, C.R.; Bruno, I.J.; Lightfoot, M.P.; Ward, S.C. The Cambridge Structural Database. *Acta Crystallogr.* **2016**, *B72*, 171–179. [[CrossRef](#)]
9. Bruno, I.J.; Cole, J.C.; Edgington, P.R.; Kessler, M.; Macrae, C.F.; McCabe, P.; Pearson, J.; Taylor, R. New software for searching the Cambridge Structural Database and visualizing crystal structures. *Acta Crystallogr.* **2002**, *B58*, 389–397. [[CrossRef](#)]
10. Grothe, E.; Meekes, H.; Vlieg, E.; ter Horst, J.H.; de Gelder, R. Solvates, salts, and cocrystals: A proposal for a feasible classification system. *Cryst. Growth Des.* **2016**, *16*, 3237–3243. [[CrossRef](#)]
11. Jin, S.; Wang, D.; Liang, S.; Chen, S. Crystal and molecular structure of two organic acid–base adducts from 2-aminopyrimidine and carboxylic acids. *J. Chem. Crystallogr.* **2012**, *42*, 759–766. [[CrossRef](#)]
12. Eshtiagh-Hosseini, H.; Yousefi, M.; Mirzaei, M. 2-Aminopyrimidinium hydrogen oxalate monohydrate. *Acta Crystallogr.* **2009**, *E65*, o2816. [[CrossRef](#)] [[PubMed](#)]
13. Miyan, L.; Adam, A.M.A.; Refat, M.S.; Alsuhaibani, A.M. 2-Aminopyrimidine-oxalic acid liquid-liquid charge-transfer interactions: Synthesis, spectroscopic characterizations, and the effect of temperature. *J. Mol. Liq.* **2022**, *365*, 120106. [[CrossRef](#)]
14. Eshtiagh-Hosseini, H.; Mahjoobizadeh, M.; Mirzaei, M. 2-Aminopyrimidinium 4-hydroxypyridinium-2,6-dicoxylate monohydrate. *Acta Crystallogr.* **2010**, *E66*, o2210.
15. Smith, G.; Wermuth, U.D.; Healy, P.C. Hydrogen bonding in proton-transfer compounds of 5-sulfosalicylic acid with *ortho*-substituted monocyclic hetroaromatic Lewis bases. *J. Chem. Crystallogr.* **2006**, *36*, 841–849. [[CrossRef](#)]

16. Smith, G.; Wermuth, U.D.; Healy, P.C.; White, J.M. Structure-making with 3,5-dinitrosalicylic acid. II.* The proton-transfer compounds of 3,5-dinitrosalicylic acid with the monocyclic heteroaromatic amines. *Aust. J. Chem.* **2003**, *56*, 707–713. [[CrossRef](#)]
17. Kobayashi, K.; Shirasaka, T.; Yamaguchi, K.; Sakamoto, S.; Horn, E.; Furukawa, N. Molecular capsule constructed by multiple hydrogen bonds: Self-assembly of cavitated tetracarboxylic acid with 2-aminopyrimidine. *Chem. Commun.* **2000**, 41–42. [[CrossRef](#)]
18. Skovsgaard, S.; Bond, A.D. Co-crystallization of benzoic acid derivatives with *N*-containing bases in solution and by mechanical grinding: Stoichiometric variants, polymorphism and twinning. *CrystEngComm* **2009**, *11*, 444–453. [[CrossRef](#)]
19. Lynch, D.E.; Smith, G.; Freney, D.; Byriel, K.A.; Kennard, H.L. Molecular cocrystals of carboxylic acids. XV* Preparation and characterization of heterocyclic base adducts with a series of carboxylic acids, and the crystal structures of the adducts of 2-aminopyrimidine with 2,6-dihydroxybenzoic acid, 4-aminobenzoic acid, phenoxyacetic acid, (2,4-dichlorophenoxy)acetic acid, (3,4-dichloro)phenoxyacetic acid and salicylic acid, and 2-aminopyridine with 2,6-dihydroxybenzoic acid. *Aust. J. Chem.* **1994**, *47*, 1097–1115.
20. Lynch, D.E.; Barfield, J.; Frost, J.; Antrobus, R.; Simmons, J. Conformational comparisons between phenoxyacetic acid derivatives in adducts and those in the free form. Part 2. *Cryst. Eng.* **2003**, *6*, 109–122. [[CrossRef](#)]
21. Ostasz, A.; Łyszczek, R.; Mazur, L.; Tarasiuk, B. Co-crystal formation between 2-amino-4,6-dimethylpyrimidine and a new *p*-xylylene-bis(thioacetic) acid. *CrystEngComm* **2014**, *16*, 10262–10272. [[CrossRef](#)]
22. Admond, D.A.; Sinha, A.S.; Khandavilli, U.B.R.; Maguire, A.R.; Lawrence, S.E. Design and synthesis of ternary cocrystals using carboxyphenols and two complementary acceptor compounds. *Cryst. Growth Des.* **2016**, *16*, 59–69. [[CrossRef](#)]
23. Zong, Y.; Shao, H.; Pang, Y.; Wang, D.; Liu, K.; Wang, L. Multicomponent hydrogen-bonding organic solids constructed from 6-hydroxy-2-naphthoic acid and *N*-heterocycles: Synthesis, structural characterization and synthon discussion. *J. Mol. Struct.* **2016**, *1115*, 187–198. [[CrossRef](#)]
24. Singh, M.P.; Tarai, A.; Baruah, J.B. Neuytal, zwitterions, ionic forms of 5-aminoisophthalic acid in cocrystals, salts and their optical properties. *ChemistrySelect* **2019**, *4*, 5427–5436. [[CrossRef](#)]
25. Thirumurugan, R.; Anitha, K. Experimental and theoretical investigations on a hydrous organic salt of 2,4,6-triaminopyrimidine-1,3-dium L-tartrate monohydrate (TTM). *J. Mol. Struct.* **2021**, *1237*, 130368. [[CrossRef](#)]
26. Sangavi, M.; Kumaraguru, N.; McMillen, C.D.; Butcher, R.J. Supramolecular interactions in some organic hydrated 2,4,6-triaminopyrimidinium carboxylate and sulfate salts. *Acta Crystallogr.* **2023**, *C79*, 435–442. [[CrossRef](#)]
27. Abidi, S.S.A.; Azim, Y.; Gupta, A.K.; Pradeep, C.P. Cocrystals of indole-3-acetic acid and indole-3-butyric acid: Synthesis, structural characterization and Hirshfeld surface analysis. *J. Mol. Struct.* **2018**, *1166*, 202–213. [[CrossRef](#)]
28. Mohana, M.; Muthiah, P.T.; McMillen, C.D.; Butcher, R.J. Supramolecular interactions in salts/cocrystals involving pyrimidine derivatives of sulfonate/carboxylic acid. *Acta Crystallogr.* **2023**, *C79*, 61–67. [[CrossRef](#)]
29. Xing, P.; Li, Q.; Li, Y.; Wang, K.; Zhang, Q.; Wang, L. Organic salts formed by 2,4,6-triaminopyrimidine and selected carboxylic acids via variety of hydrogen bonds: Synthons cooperation, and crystal structures. *J. Mol. Struct.* **2017**, *1136*, 59–68. [[CrossRef](#)]
30. Mapp, L.K.; Coles, S.J.; Aitipamula, S. Novel solid forms of Ionidamine: Crystal structures and physicochemical properties. *CrystEngComm* **2017**, *19*, 2925–2935. [[CrossRef](#)]
31. Li, Z.; Li, Y.; Du, F. Crystal structure of 2,4,6-pyrimidinetriamine-trifluoroacetate(1:1), $C_4H_8N_5^+C_2F_3O_2^-$, $C_6H_8F_3N_5O_2$. *Z. Kristallogr. NCS* **2012**, *227*, 519–520.
32. Garg, U.; Azim, Y.; Kar, A.; Pradeep, C.P. Cocrystals/salt of 1-naphthaleneacetic acid and utilizing Hirshfeld surface calculations for acid–aminopyrimidine synthons. *CrystEngComm* **2020**, *22*, 2978–2989. [[CrossRef](#)]
33. Pedireddi, V.R.; Chatterjee, S.; Ranganathan, A.; Rao, C.N.R. A study of supramolecular hydrogen bonded complexes formed by aliphatic dicarboxylic acids with azaaromatic donors. *Tetrahedron* **1998**, *54*, 9457–9474. [[CrossRef](#)]
34. Sienkiewicz-Gromiuk, J.; Tarasiuk, B.; Mazur, L. New organic single crystal of (benzylthio)acetic acid: Synthesis, crystal structure, spectroscopic (ATR-FTIR, 1H and ^{13}C NMR) and thermal characterization. *J. Mol. Struct.* **2016**, *1110*, 65–71. [[CrossRef](#)]
35. Sienkiewicz-Gromiuk, J.; Drzewiecka-Antonik, A. The first noncovalent-bonded supramolecular frameworks of (benzylthio)acetic acid with proline compounds, isonicotinamide and tryptamine. *Molecules* **2022**, *27*, 8203. [[CrossRef](#)] [[PubMed](#)]
36. *CrysAlis PRO*, v.1.171.37.35g; Agilent Technologies Ltd.: Oxford, UK, 2014.
37. Sheldrick, G.M. A short history of SHELX. *Acta Crystallogr.* **2008**, *A64*, 112–122. [[CrossRef](#)] [[PubMed](#)]
38. Sheldrick, G.M. Crystal structure refinement with SHELXL. *Acta Crystallogr.* **2015**, *C71*, 3–8.
39. Farrugia, L.J. WinGX and ORTEP for Windows: An update. *J. Appl. Cryst.* **2012**, *45*, 849–854. [[CrossRef](#)]
40. Macrae, C.F.; Sovago, I.; Cottrell, S.J.; Galek, P.T.A.; McCabe, P.; Pidcock, E.; Platings, M.; Shields, G.P.; Stevens, J.S.; Towler, M.; et al. Mercury 4.0: From visualization to analysis, design and prediction. *J. Appl. Crystallogr.* **2020**, *53*, 226–235. [[CrossRef](#)]
41. Singaravelan, K.; Chandramohan, A.; Madhankumar, S.; Enoch, M.V.; Vinitha, G. Structural characterization, computational and biological studies of a new third order NLO (1:1) organic adduct: 2-Aminopyrimidine:3-nitrophthalic acid. *J. Mol. Struct.* **2019**, *1194*, 57–65. [[CrossRef](#)]
42. Sienkiewicz-Gromiuk, J. DFT approach to (benzylthio)acetic acid: Conformational search. Molecular (monomer and dimer) structure, vibrational spectroscopy and some electronic properties. *Spectrochim. Acta A* **2018**, *189*, 116–128. [[CrossRef](#)] [[PubMed](#)]
43. Prabavathi, N.; Nilufer, A.; Krishnakumar, V.; Akilandeswari, L. Spectroscopic, electronic structure and natural bond analysis of 2-aminopyrimidine and 4-aminopyrazolo[3,4-d]pyrimidine: A comparative study. *Spectrochim. Acta A* **2012**, *96*, 226–241. [[CrossRef](#)] [[PubMed](#)]
44. Rospenk, M.; Koll, A. Self-assembly of 2-aminopyrimidines in nonpolar solvents. *J. Mol. Struct.* **2007**, *844–845*, 232–241. [[CrossRef](#)]

45. Fu, W.-W.; Liu, Y.; Huang, G.; Zhu, X.-M. 4,6-dimethylpyrimidin-2-amine. *Acta Crystallogr.* **2013**, *E69*, o32. [[CrossRef](#)]
46. Lin, C.-H.; Guo, H.-M.; Jian, F.-F. Crystal structure of 2-amino-4,6-dimethylpyrimidine hydrate, $(C_6H_9N_3)_{10} \cdot H_2O$. *Z. Kristallogr. NCS* **2008**, *223*, 511–512. [[CrossRef](#)]
47. Li, Z.; Huang, J.; Meng, A.; Zheng, B. Crystal Structure, energy band and optical properties of benzoic acid—2,amino-4,6-dimethylpyrimidine (1:1) co-crystals. *J. Struct. Chem.* **2010**, *51*, 53–59. [[CrossRef](#)]
48. Sundaraganesan, N.; Joshua, B.D.; Meganathan, C.; Sebastian, S. Vibrational spectroscopic studies supported by HF/DFT calculations of 2,4,6-triaminopyrimidine. *Indian J. Chem.* **2008**, *A47*, 821–829.

Disclaimer/Publisher's Note: The statements, opinions and data contained in all publications are solely those of the individual author(s) and contributor(s) and not of MDPI and/or the editor(s). MDPI and/or the editor(s) disclaim responsibility for any injury to people or property resulting from any ideas, methods, instructions or products referred to in the content.